International Journal of Structural Analysis & Design– IJSAD
Volume 2: Issue 1 [ISSN : 2372-4102]
Publication Date : 30 April, 2015

Remedy for the Improvement of Seismic Resistance Capacity of a T-stub Connection Under Axial Cyclic Loading

Yang Jae-guen, Kim Joo-woo, Kim Woo-bum, Lee Myung-jae, Lee Hyung-dong, Lee Jae-yoon

Shape memory alloys are new materials that provide excellent superelastic capacity and shape memory capability due to phase changes of austenite and martensite. In recent years, the shape memory alloys have been applied to steel-structure buildings in the form of dampers, steel rods and wires, thereby increasing buildings' seismic performance.

This study was designed to seek ways to improve the seismic performance of T-stub connections subjected to axial cyclic loading. In a related move, this study sought to investigate changes in the energy dissipation capacity and residual deformation of the connections due to changes in the geometric shape of the T-stub. Towards this end, a three-dimensional nonlinear finite element analysis was performed with respect to the T-stub connections using SMA.

***Keywords*—T-stub, shape memory alloy, residual deformation, energy dissipation capacity, nonlinear finite element analysis**

Yang Jae-guen *(Corresponding aouthor)*
Department of Architectural Engineering / Inha University
Republic of Korea

Kim Joo-woo,
Department of Architectural Engineering / Semyun University
Republic of Korea

Kim Woo-bum
Department of Architectural Engineering / Kongju University
Republic of Korea

Lee Myung-jae
Department of Architectural Engineering / Chung-Ang University
Republic of Korea

Lee Hyung-dong,
Department of Architectural Engineering / Inha University
Republic of Korea

Lee Jae-yoon
Department of Architectural Engineering / Inha University
Republic of Korea

I. Introduction

T-stub connections display different behavior characteristics depending on changes in the thickness of the T-stub, the diameter and number of fasteners and gauge distance of the fasteners. T-stub connections subjected to axial tensile loads show three types of failure modes as shown in Figure 1 according to the geometric parameter α` defined by the equation (1). In addition, T-stub connections exert different energy dissipation capacity according to the geometric parameter α` under cyclic loading. In general, for T-stub connections with a relatively large α`value, the energy dissipation capacity is affected by plastic deformation after the flexural yielding of T-stub flanges. On the other hand, in the case of T-stub connections with a relatively small α`value, the energy dissipation capacity is affected by the yielding or fracture of fasteners.

The SMAs with excellent superelastic capacity and shape memory capability exhibit a stress-strain-temperature relationship curve as in Figure 2 depending on the combination of shape alloys and changes in the temperature of austenite and martensite. Accordingly, this study attempted to identify the energy dissipation capacity and residual deformation of the connections according to the changes in α`values by selecting the T-stub and applying SMA to improve the seismic performance of T-sub connections. To this end, T-stub connections using SMA were modeled using commercial software including ABAQUS (ver. 6.10.1), and a three-dimensional nonlinear finite element analysis was performed.

$$\alpha' = \frac{1}{\delta(1+\rho)}\left\{\left(\frac{t_c}{t_f}\right)^2 - 1\right\} \quad (1)$$

$$t_c = \sqrt{\frac{8B_0 b'}{pF_y}} \quad (2)$$

$$\rho = \frac{b'}{a'} \quad (3)$$

$$\delta = 1 - \frac{d'}{p} \quad (4)$$

$$a' = a + \frac{d_b}{2} \quad (5)$$

$$b' = b - \frac{d_b}{2} \quad (6)$$

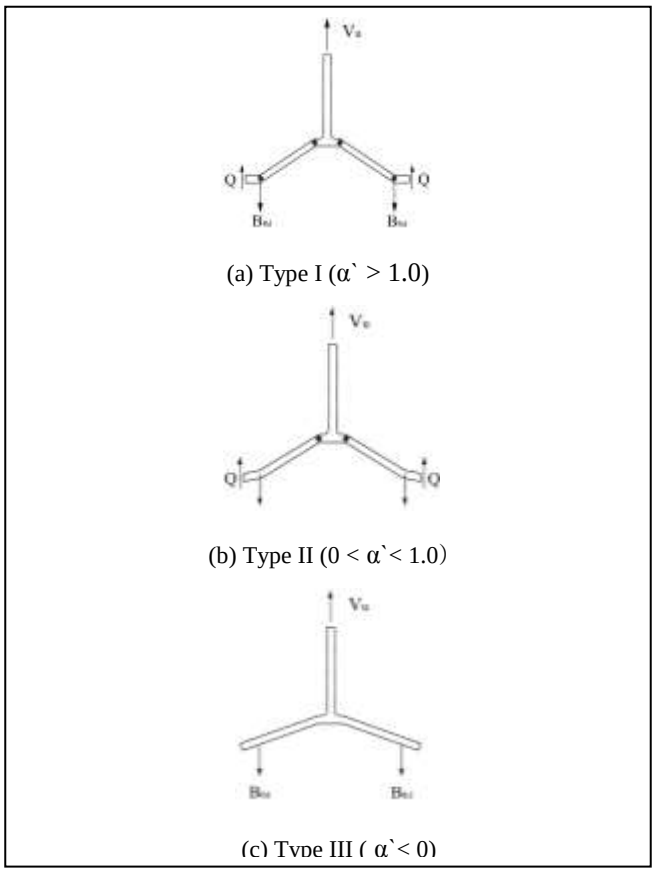

Figure 1. Failure modes of a T-stub connection due to the changes of α`

II. Three-dimensional nonlinear finite element analysis of T-stub connections using SMA under axial cyclic loading

A. *Finite element analysis of T-stub connections using SMA*

Three analysis models of T-stub connections were modeled to determine the energy dissipation capacity and residual deformation of T-stub connections using SMA under axial cyclic loading. The material properties of SMA T-stub and F10T-M20 high-tension bolts applied to the finite element analysis are summarized in Tables Ⅰ and Ⅱ. As shown in Figure 3 and Table Ⅲ, analysis models of the T-stub connections were induced to lead the connection failure resulting from the yield and fracture of high-tension bolts as well as the flexural yielding of T-stub flange or fillet. For the finite element analysis, the bearing and contact between members, and introduction of the pretension of high-tension bolts were included. Table Ⅳ shows the ABAQUS options applied in the finite element analysis. The cyclic loading acting on T-stub connections was applied at the end of the T-stub stem in the form of displacement control as shown in Figure 4.

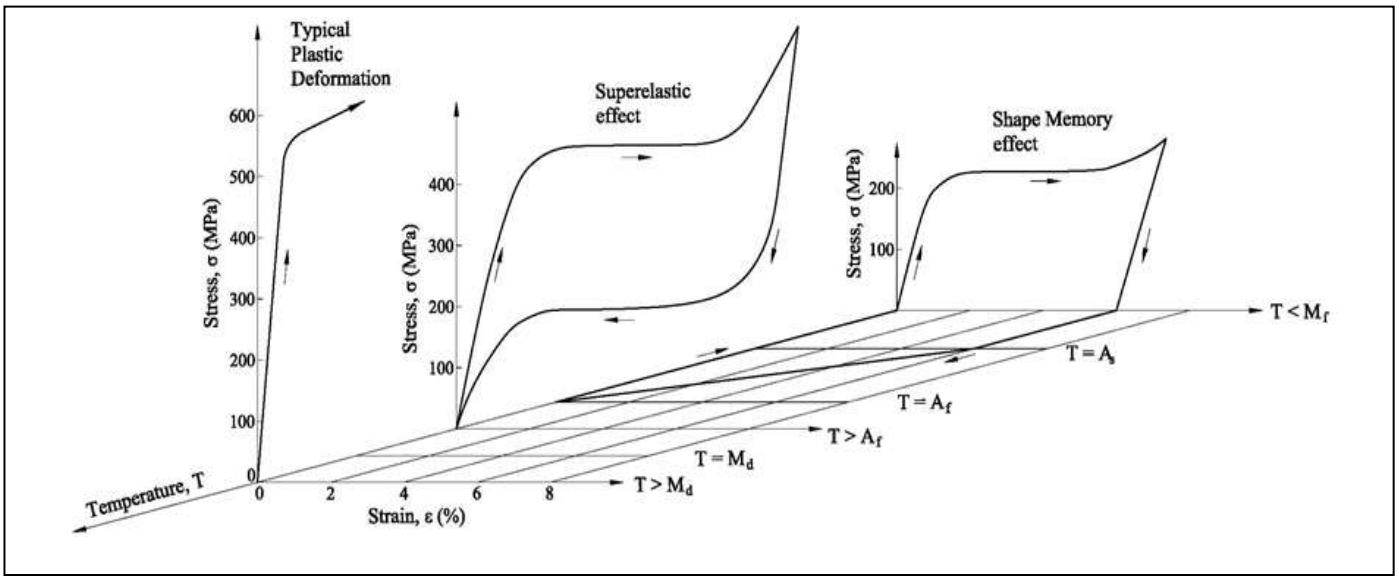

Figure 2. Stress-strain relationship and shape memory effect of NiTi SMA

TABLE I. MATERIAL PROPERTIES OF SMA T-STUB USED IN THE FINITE ELEMENT ANALYSIS

Material variables	*Input values*
E^A **: Elastic modulus of austenite**	**70,000 MPa**
E^M **:Elastic modulus of martensite**	**30,000 MPa**
υ **: Poisson's ratio**	**0.33**
M^s **: Martenite finish temperature**	**253 K (-20.15℃)**
M^f **: Martenite start temperature**	**244 K (-29.15℃)**
A^s **: Austenite start temperature**	**264 K (-9.15℃)**
A^f **: Austenite finish temperature**	**277 K (4.15℃)**
T_{test} **: Current experimental temperature**	**293 K (19.85℃)**
H **: Maximum transformation strain**	**0.05**

TABLE II. MATERIAL PROPERTIES OF F10T-M20 HIGH-TENSION BOLTS

F_y (N/mm^2)	F_u (N/mm^2)	E (N/mm^2)	ε_y	ε_u
900	**1,000**	**205,000**	**0.0015854**	**0.0115854**

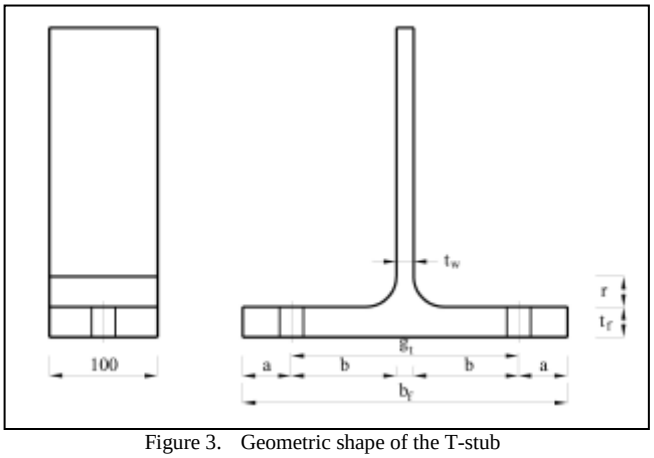

Figure 3. Geometric shape of the T-stub

TABLE III. GEOMETRIC PARAMETERS OF T-STUB

SPECIMEN	b_f (mm)	t_w (mm)	t_f (mm)	g_t (mm)	r (mm)	a (mm)	b (mm)	α'
G210-T15-B300	300	15	15	210	22	45	97.5	7.32
G210-T21-B300	300	13	21	210	22	45	98.5	3.51
G210-T28-B300	300	16	28	210	28	45	97	1.74

TABLE IV. ABAQUS OPTIONS APPLIED IN ANALYSIS

Contacts	*Command*	*Options*		
Washer contacts	**Constraint**	**Tie**		
T-stub – T-stub	**Contact**	**Finite sliding**	**Allow separation after contact**	**Adjust only to remove over closure**
T-stub – high-tension bolts				
Nuts – high-tension bolts		**Small sliding**		

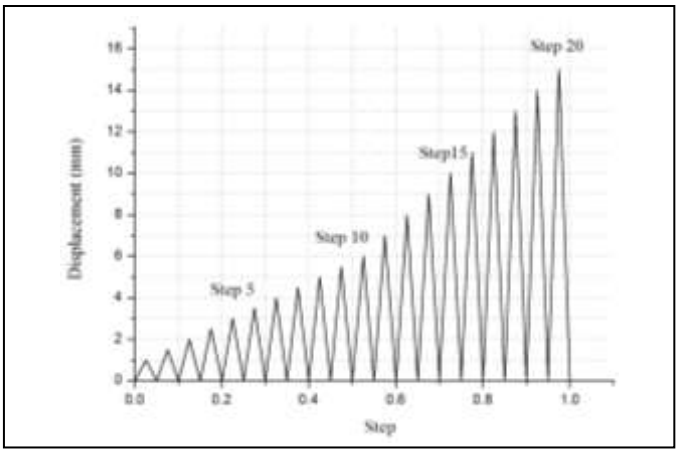

Figure 4. Loading protocol of a T-stub analysis model.

B. *Finite element analysis results of T-stub connections using SMA*

The geometric parameter values α` of the T-stub connections using SMA were 7.32, 3.51 and 1.74. In this case, it can be predicted that the T-stub displays failure modes of Figure 1(a) and 1(b). Therefore, stress distribution and deformation patterns that occur in the T-stub flanges and high-tension bolts were carefully determined. Figures 5, 6 and 7 show stress distribution and load-displacement hysteresis loops for each T-stub analysis model obtained through the three-dimensional nonlinear finite element analysis.

In the case of G210-T28-B300 model (α`=1.74), stress concentrations where the high-tension bolts come in contact with T-stub flange were not clearly observed. However, T-stub fillets showed distinct stress concentrations and exceeded the yield stress to some extent. Meanwhile, stress concentrations also occurred in F10T-M20 high-tension bolts, and they exceed the yield stress of the high-tension bolts. Therefore, it can be determined that tensile fracture of the high-tension bolts occurred.

G210-T21-B300 model (α`=3.51) showed more distinct stress concentrations where the high-tension bolts come in

contact with T-stub flange than the G210-T21-B300 model (α`=1.74). In addition, stress concentrations of T-stub fillets were not more clearly observed than the G210-T28-B300 model, however they exceeded the yield stress to some extent. And, stress concentrations of F10T-M20 high-tension bolts did not clearly occur compared to those of G210-T28-B300 model (α′=1.74).

G210-T15-B300 model (α`=7.32) showed more distinct stress concentrations where the high-tension bolts come in contact with T-stub flange than G210-T21-B300 model (α`=3.51). In addition, stress concentrations of T-stub fillets were not more clearly observed than G210-T28-B300 model. However, they exceeded the yield stress to some extent. And, stress concentrations of F10T-M20 high-tension bolts did not Cclearly occur compared to those of G210-T28-B300 model (α`=1.74).

Load-displacement hysteresis loops for each analysis model obtained through the finite element analysis of the T-stub connections using SMA are shown in Figures 5, 6 and 7. As identified in the load-displacement hysteresis loops for each connection, the residual deformation due to load application almost did not occur in all connections. As summarized in Table Ⅴ, the total energy dissipation capacity of each step, which corresponds to the internal area of load-displacement hysteresis loops, increased as the geometric parameter values α` decreased.

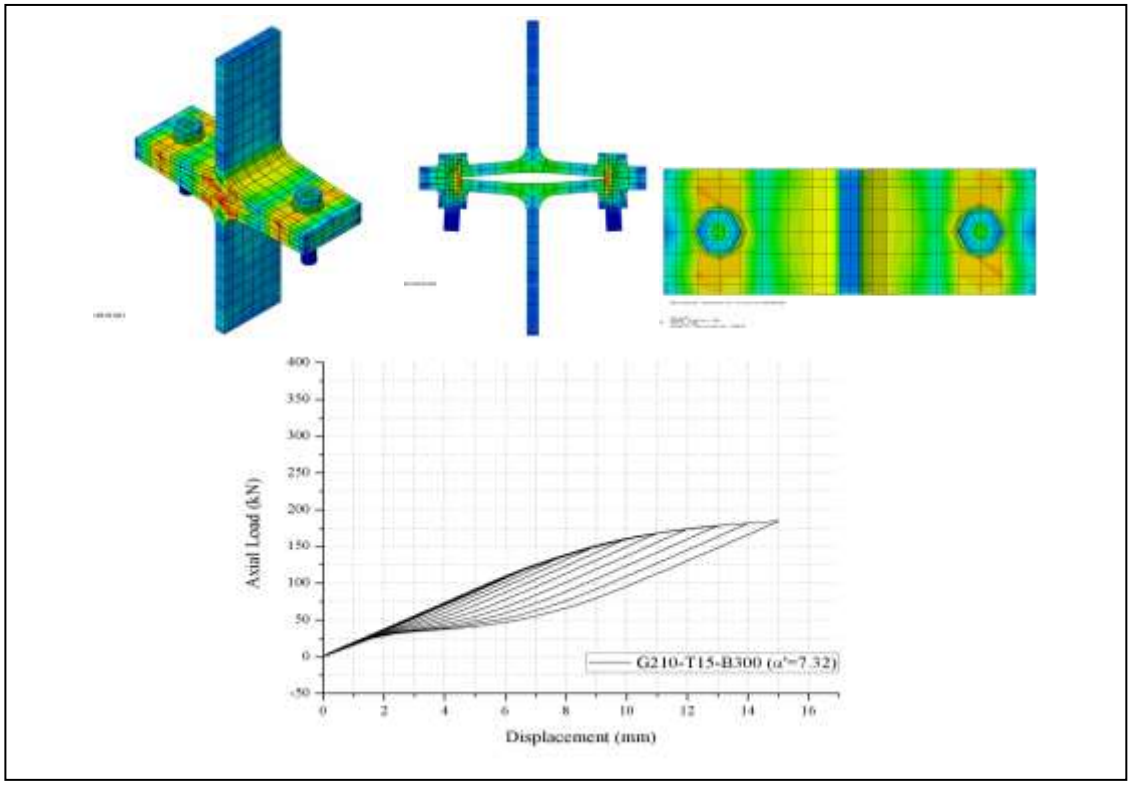

Figure 5. Stress distribution and Load-displacement curve of G210-T15-B300 (α`=7.32)

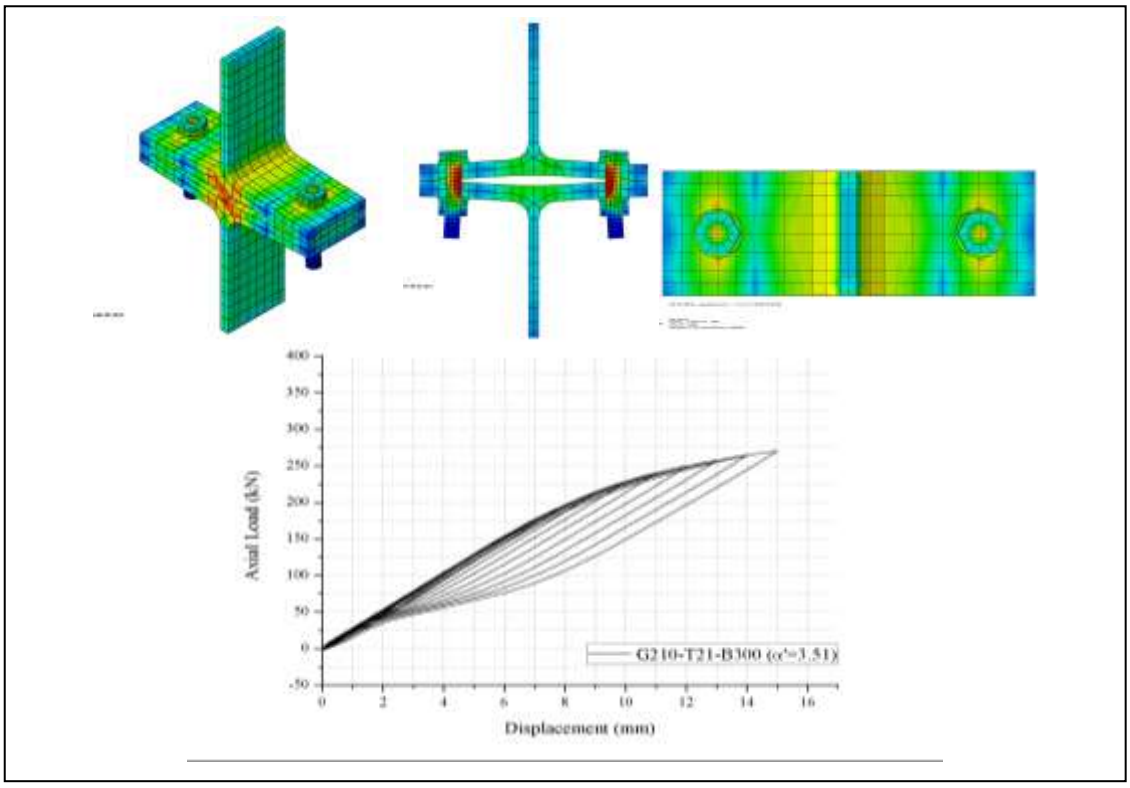

Figure 6. Stress distribution and Load-displacement curve of G210-T21-B300 (α`=3.51)

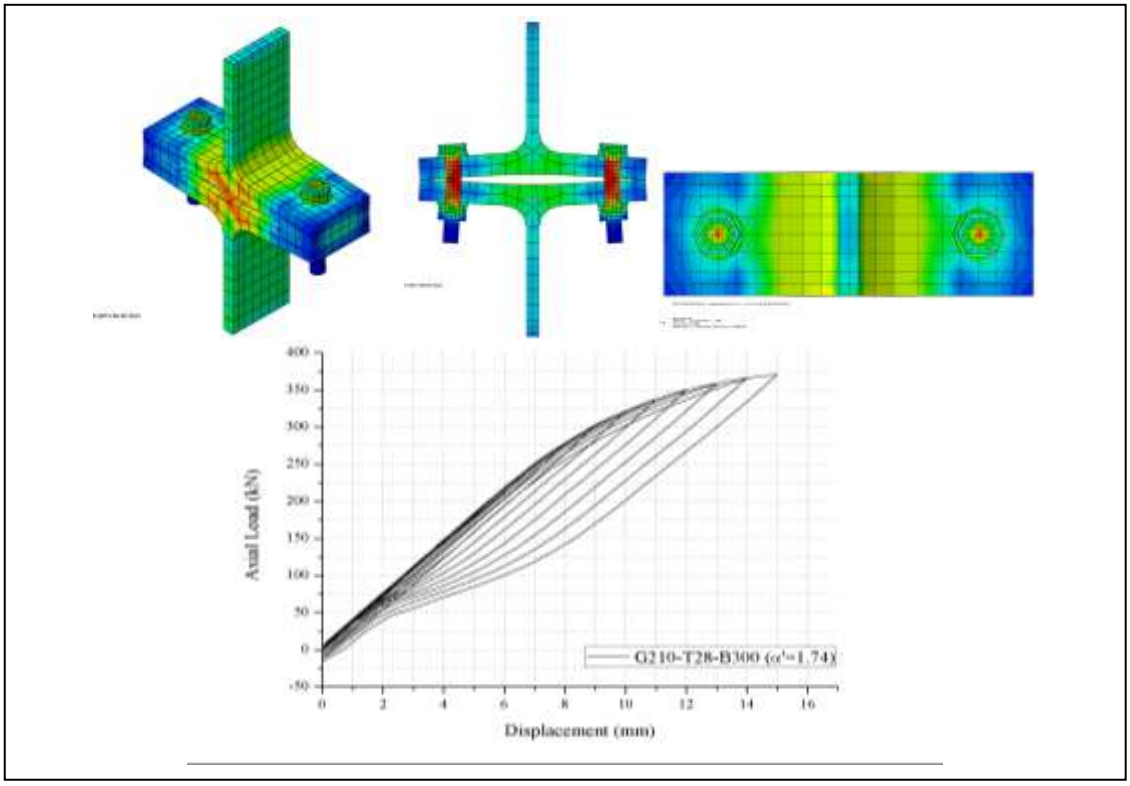

Figure 7. Stress distribution and Load-displacement curve of G210-T28-B300 (α`=1.74)

TABLE V. COMPARISON OF THE ENERGY DISSIPATION CAPACITIES

Cycle	*G210-T15-B300 (α`=7.32)* *(kN·mm)*	*G210-T21-B300 (α`=3.51)* *(kN·mm)*	*G210-T28-B300 (α`=1.74)* *(kN·mm)*
1	0.0246	0.0342	0.0977
2	0.0644	0.0646	0.2642
3	0.1842	0.1681	0.4417
4	0.3533	0.6162	0.7905
5	0.6452	0.4482	1.1882
6	0.9168	0.6899	1.7500
7	1.1303	0.9961	2.3914
8	1.3717	1.4012	3.1557
9	1.8139	2.1959	4.0480
10	2.4738	2.6425	5.0848
11	4.6507	7.3336	8.5516
12	17.3216	19.2971	28.0220
13	41.7719	48.7644	72.9375
14	75.9851	92.5108	137.1222
15	127.6421	155.7496	234.8537
16	195.9540	242.1948	352.1488
17	277.8031	341.1114	492.8959
18	372.7833	445.4425	643.7063
19	476.6949	553.2100	800.4749
20	586.4266	662.1940	956.1001
$E_{D,total}$	2,186.01	2,577.07	3,746.03

III. Conclusion

In this study, T-sub connections using SMA were selected to improve the seismic performance of T-stub connections. This study sought to investigate energy dissipation capacity and residual deformation according to changes in α` of T-stub connections using SMA. The following conclusions were derived from the results of this study.

1) SMA T-stub connections with α` values =7.32, 3.51 and 1.74 suffered from failure due to the plastic deformation after flexural yielding of T-stub fillets. In addition, the tensile fracture of the F10T-M20 high-tension bolts occurred when α` valve is equal to 1.74.
2) As α` values decreased, the energy dissipation capacity of T-stub connections using SMA increased. This is attributed to the effects of the superelastic capacity and shape memory capability of SMA.
3) As for the T-stub connections using SMA considered in this study, the residual deformation due to load application almost did not occur, indicating that improving the seismic performance of connections helps

Acknowledgment

This study is a part of the results of a research project conducted by the National Research Foundation of Korea (Project Number: **NRF-2013R1A2A2A07067970**). The authors of this paper extend their sincere gratitude to the said institution.

References

[1] Kulak, G. L., J.W. Fisher and J.H.A. Struik, 1987, Guide to Design Criteria for Bolted and Riveted Joints, Second Edition, John Wiley & Sons, New York,

[2] R. DesRoches at al. (2004), Cyclic Properties of Superelastic Shape Memory Alloy Wires and Bars, Journal of Structual Engineering, JANUARY, ASCE 38-46.

[3] A. Abolmaali et al. (2006), Hysteresis behavior of t-stub connections with superelastic shape memory fasteners, Journal of Constructional Steel Research, 62 831–838

[4] Yang Jae-Guen, Baek Min-Chang, Lee Jae-yun, Lee, Hyung Dong. (2014), Energy Dissipation Capacity of the T-stub Fastened by SMA bars, Journal of Korean Society of Steel Construction, Vol.26 231-240